Journal of Structural Biology xxx (2015) xxx–xxx

Contents lists available at ScienceDirect

Journal of Structural Biology

journal homepage: www.elsevier.com/locate/yjsbi

The PKA regulatory subunit from yeast forms a homotetramer: Low-resolution structure of the N-terminal oligomerization domain

Nicolás González Bardeci [a], Julio J. Caramelo [a,b], Donald K. Blumenthal [c], Jimena Rinaldi [b], Silvia Rossi [a], Silvia Moreno [a,*]

[a] Departamento de Química Biológica, IQUIBICEN-CONICET, Facultad de Ciencias Exactas y Naturales, Universidad de Buenos Aires, C1428EGA Buenos Aires, Argentina
[b] Fundación Instituto Leloir, IIBBA-CONICET, C1405BWE Buenos Aires, Argentina
[c] Department of Pharmacology & Toxicology, University of Utah, Salt Lake City, UT 84112, USA

ARTICLE INFO

Article history:
Received 10 August 2015
Received in revised form 13 October 2015
Accepted 6 December 2015
Available online xxxx

Keywords:
Protein kinase A
Regulatory subunit
Bcy1
Saccharomyces cerevisiae
D/D domain

ABSTRACT

The cAMP dependent protein kinase (PKA) is a key enzyme involved in many cellular processes in eukaryotes. In mammals, the regulatory (R) subunit localises the catalytic (C) subunit to specific subcellular sites through the interaction of its N-terminal homodimeric docking and dimerization (D/D) domain with specific scaffold proteins. The structure of the D/D domain has been extensively studied in mammals, but there is little information from non-mammalian species. In this work, we present the structural analysis of the D/D domain of Bcy1, the R subunit of PKA from *Saccharomyces cerevisiae*. Using chemical crosslinking experiments and static light scattering measurements we found that this R subunit forms a tetramer in solution, unlike its dimeric mammalian counterparts. We determined that the D/D domain is responsible for this unusual oligomeric state. Using biophysical techniques including size-exclusion chromatography, sucrose gradient sedimentation, small angle X-ray scattering (SAXS), and circular dichroism, we performed a detailed structural characterization of the tetrameric D/D domain of Bcy1. We used homology modelling in combination with computer-aided docking methods and *ab initio* SAXS modelling methods to develop structural models for the D/D domain tetramer. The models consist of two homodimers with a canonical D/D domain fold that generate a dimer of dimers with novel putative interaction surfaces. These findings indicate that the oligomerization states of PKA R subunits is more diverse than previously thought, and suggest that this might allow some forms of PKA to interact with a wide range of intracellular partners.

© 2015 Elsevier Inc. All rights reserved.

1. Introduction

The cAMP-protein kinase A (PKA) signalling pathway is involved in the regulation of a great diversity of fundamental cellular processes in most eukaryotic organisms, including mammals and yeast (Gancedo, 2013). PKA is a serine/threonine kinase that serves as a prototype for the protein kinase superfamily in the study of different aspects of signal transduction processes. It is composed of two different types of subunits: a catalytic (C) subunit, which performs the phosphate transfer reaction, and a regulatory (R) subunit, responsible for providing regulation of the C subunit activity at many different levels (Pidoux and Tasken, 2010; Taylor et al., 2005).

The classical model of PKA activation involves a catalytically inactive state, which exists in the absence of cAMP, and is represented by a heterotetrameric holoenzyme, R_2C_2, and an active state, represented by free C subunits, which is achieved as a consequence of the increase of the intracellular levels of cAMP in response to specific extracellular stimuli. The inactive holoenzyme is composed of a dimer of R subunits and two C subunits. When intracellular cAMP levels rise, each R subunit in the holoenzyme binds two molecules of the second messenger, triggering conformational changes which loosens the interaction with C, and finally

Abbreviations: AKAPs, A-Kinase anchoring proteins; C, catalytic (subunit); CBD, cAMP binding domain; CD, circular dichroism; D/D domain, dimerization and docking domain; D_{max}, maximum intraparticle distance; EGS, ethylene glycol bis [succinimidylsuccinate]; IS, inhibitory site; PKA, protein kinase A; *R*, regulatory (subunit); R_g, radius of gyration; R_s, Stokes radius; *s*, sedimentation coefficient; SAXS, small-angle X-ray scattering; SEC, size-exclusion chromatography; SLS, static light scattering.

* Corresponding author at: Departamento de Química Biológica, Facultad de Ciencias Exactas y Naturales, Universidad de Buenos Aires, Intendente Güiraldes 2160, Ciudad Universitaria, Pabellón 2, Piso 4, C1428EGA Buenos Aires, Argentina.
E-mail address: smoreno@qb.fcen.uba.ar (S. Moreno).

http://dx.doi.org/10.1016/j.jsb.2015.12.001
1047-8477/© 2015 Elsevier Inc. All rights reserved.

Please cite this article in press as: González Bardeci, N., et al. The PKA regulatory subunit from yeast forms a homotetramer: Low-resolution structure of the N-terminal oligomerization domain. J. Struct. Biol. (2015), http://dx.doi.org/10.1016/j.jsb.2015.12.001

dissociates the complex into two free C subunits and a dimer of cAMP-bound R subunits (Johnson et al., 2001). Today it is recognised that the activation mechanism is more complex than this, and that the substrate plays an important role in the activation process (Vigil et al., 2004a).

An important level of regulation of the specificity of PKA activity *in vivo* is achieved by the interaction of the holoenzyme with AKAPs (A-kinase anchoring proteins), which are scaffold proteins responsible for determining the subcellular localization of the holoenzyme. To date, AKAPs have been described in a restricted group of organisms including mammals (Burgers et al., 2012), *Drosophila* (Hadad et al., 2011) and *C. elegans* (Angelo and Rubin, 1998). Many of the physiologically most relevant spatio-temporal effects of PKA signalling are mediated by AKAPs (Tasken and Aandahl, 2004; Welch et al., 2010).

The structural features of the C and R subunits have been extensively studied in mammals. In this system, four isoforms of the R subunit exist: RIα, RIβ, RIIα and RIIβ. They are all proteins of ~400 amino acids, which share the same domain organisation (Fig. 1a): an N-terminal region responsible for dimerization and for docking to AKAPs (D/D domain), a linker region which contains an inhibitory site (IS) that occupies the catalytic pocket of the C subunit in the holoenzyme, and two cAMP binding domains located at the C-terminus (Taylor et al., 2005). RI and RII dimers differ in structural aspects regarding global conformation (Vigil et al., 2004b), structure of the D/D domains (Banky et al., 2003; Newlon et al., 1999) and the presence of an autophosphorylation site in the IS (Canaves and Taylor, 2002). The structure of the region corresponding to the cAMP binding domains has been studied both in mammals (Su et al., 1995) and yeast (Rinaldi et al., 2010). An exhaustive phylogenetic study of these domains has also been reported (Canaves and Taylor, 2002). However, little attention has been paid to the structure of the D/D domain in non-mammalian systems.

The D/D domain from mammalian R subunits is a compact domain which folds into an antiparallel X-type four helix bundle structure; each protomer contributes to the dimer a sequence of ~50 amino acids which constitutes a helix-turn-helix motif. A core of highly conserved hydrophobic residues constitutes the dimer interface (Banky et al., 2003; Newlon et al., 1999). A hydrophobic groove at the surface of the D/D domain serves as the platform for AKAP binding; all AKAPs harbour a ~20 amino acid amphipathic α-helix with its hydrophobic face docking to this surface (Kinderman et al., 2006; Sarma et al., 2010). Several works have defined the limits of the region responsible for dimerization and docking to AKAPs for the different isoforms of the R subunit (Pidoux and Tasken, 2010). Mutagenesis studies (Banky et al., 1998; Hausken et al., 1994; Li and Rubin, 1995) and high-resolution structural studies (Banky et al., 2003; Newlon et al., 1999) have identified the amino acids in different D/D domain isoforms critical for dimerization and binding to AKAPs.

In *Saccharomyces cerevisiae*, PKA is involved in signal transduction events related to nutrient sensing, growth, response to stress, and other important physiological processes (Conrad et al., 2014). As in most fungal organisms, the R subunit is encoded by a single gene, *BCY1* (Toda et al., 1987). No AKAPs have been described to date in this organism nor in other fungi; however, the localization of Bcy1 is a regulated process, and this regulation is dependent on its N-terminus, since the first 48 residues of Bcy1 are necessary for its nuclear localization in cells growing in exponential phase in glucose (Griffioen et al., 2000). Moreover, it has been proposed that functional analogues of AKAPs that interact with the phosphorylated N-terminus of Bcy1 may exist (Griffioen et al., 2001). Recently our group has described novel, N-terminus-dependent interacting proteins for Bcy1 (Galello et al., 2014). Two of these proteins (Ira2 and Hsp60) were shown to colocalize *in vivo* with Bcy1 and may participate in determining its subcellular localization; however, the interaction of the N-terminus of Bcy1 with these partners seems to be quite different from the D/D domain-AKAP interaction in mammals since it relies on ionic interactions rather than hydrophobic interactions.

This report is focused on the structure of the N-terminal domain of Bcy1, as a first step in understanding its role in dimerization and the subcellular localization of the protein. We present here the first structural characterization of the D/D domain of a non-mammalian PKA R subunit. Using a combination of biophysical techniques and biochemical approaches, we show the existence of a novel tetrameric structure for this N-terminal domain. We propose a model of this structure, and discuss differences and similarities with mammalian D/D domains.

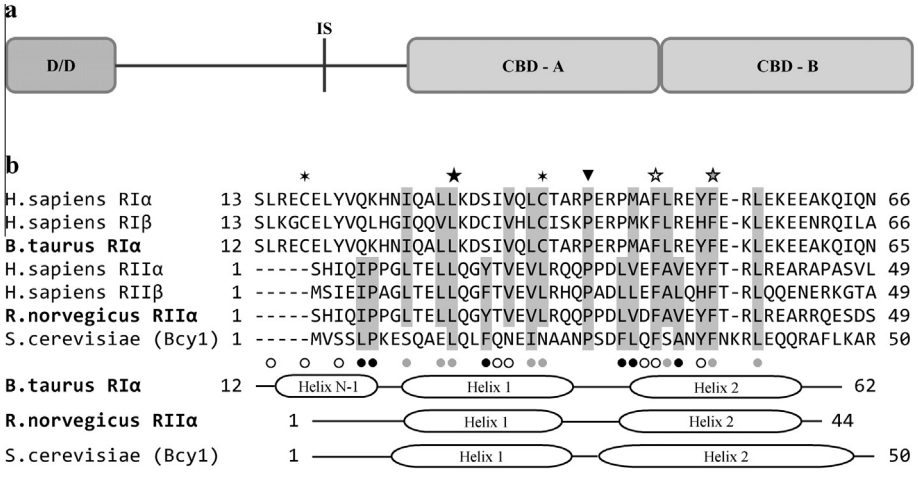

Fig. 1. Sequence analysis of D/D domains. (a) Schematic representation of the domain organisation of PKA R subunits. D/D: docking and dimerization domain; CBD: cAMP-binding domain; IS: inhibitory site. (b) Multiple sequence alignment and secondary structure of D/D domains. The black arrowhead indicates the position of the central proline. Asterisks indicate cysteine residues involved in disulphide bond formation in RIα. Stars indicate residues which disrupt dimerization of mammalian R subunits after mutation to alanine, and dots indicate residues involved in important dimer contacts as revealed by the NMR structures of RIα and RIIα. In both cases, white corresponds to RIα only, black to RIIα only, and grey to both. Conserved hydrophobic residues are highlighted in grey. White boxes in the bottom indicate α-helical regions (experimental for RIα and RIIα, and predicted for Bcy1). Proteins for which structural information is available are indicated in bold: bovine RIα (pdb code: 2EZW), and rat RIIα (pdb code: 1R2A).

Please cite this article in press as: González Bardeci, N., et al. The PKA regulatory subunit from yeast forms a homotetramer: Low-resolution structure of the N-terminal oligomerization domain. J. Struct. Biol. (2015), http://dx.doi.org/10.1016/j.jsb.2015.12.001

2. Materials and methods

2.1. Growth media and culture conditions

S. cerevisiae growth media were prepared as previously described (Sherman et al., 1986). For maintenance of plasmids YEp51-*BCY1* (Portela et al., 2001) and YEp51-Δ85*BCY1* (Galello et al., 2014), synthetic medium containing 0.67% yeast nitrogen base without amino acids, 2% glucose plus the necessary additions to fulfil auxotrophic requirements was used. To induce expression from GAL10 promoter, rich medium containing 1% yeast extract, 2% bactopeptone and 2% galactose (YPGal) was used. Typically, a 100 mL batch of a ~1 day culture in synthetic medium of *S. cerevisiae* KT 1115 strain (MATa *leu2 ura3 his3 pep4*Δ) transformed with either YEp51-*BCY1* or YEp51-Δ85*BCY1* was grown, cells were harvested, washed once to remove excess of glucose, and used to inoculate 1 L of YPGal. This culture was grown overnight for overexpression and the cells were harvested and used for protein purification.

Escherichia coli BL21-CodonPlus (DE3)-RIPL cells carrying plasmid pET32a-Bcy1-50 were grown in LB medium (0.5% yeast extract, 0.5% NaCl, 1% bactopeptone), supplemented with 100 μg/mL ampicillin and 34 μg/mL cloramphenicol for maintenance of the plasmids. For the purification of Bcy1 1-50, typically a 50 mL aliquot of an overnight grown bacterial culture was used to inoculate 1 L of media. This culture was incubated for ~2 h, and when an OD = 0.6/0.8 was reached, the overexpression of the recombinant protein was induced by addition of 0.1 mM IPTG (Sigma). After 4 h of overexpression, cells were harvested and used for protein purification.

2.2. Cloning of Bcy1 1-50

The plasmid pET32a-Bcy1-50 was engineered by inserting a DNA fragment encoding amino acids 1-50 of Bcy1 between NcoI and SacI sites in pET32a (Novagen). The oligonucleotides forward: 5′-GACGACAAGGCCATGGTATCTTCTTTGCCCAAG-3′ and reverse: 5′-CAAGCTTGTCGACG-GTTACCTGGCCTTGAGGAACG-3′ were used to amplify by PCR the appropriate region of *BCY1*, using as template the plasmid YEp51-*BCY1* (Portela et al., 2001). The reverse primer introduces an artificial stop codon immediately after amino acid 50, thus generating a fusion protein which contains at the N-terminus of the fragment Bcy1 1-50 a thioredoxin tag, a polihistidine tag, an S-tag, and an enterokinase cleavage site for tag removal. Cloning of the amplified fragment into the vector digested with both NcoI and SacI (Promega) was achieved using the InFusion cloning system (Clontech). The sequence of the coding region was verified by DNA sequencing. The recombinant vector was transformed into *E. coli* BL21-CodonPlus (DE3)-RIPL cells for further expression of the fusion protein.

2.3. Protein expression and purification

Bcy1 WT and Bcy1 Δ1-85 were produced using a modified version of a previously reported procedure (Galello et al., 2014). *S. cerevisiae* KT 1115 strain transformed with either YEp51-*BCY1* or YEp51-Δ85*BCY1*, which express the corresponding proteins under GAL10 promoter, were used as the protein sources. The cells were resuspended in lysis buffer (20 mM phosphate, 100 mM NaCl, 10 mM DTT, 5 mM EDTA, pH 7.4) supplemented with protease inhibitor cocktail (Roche), and whole cell lysates were obtained by disruption of the cell suspension with glass beads. Cellular debris was pelleted by centrifugation and the clarified whole cell lysates were incubated overnight at 4 °C with N6-cAMP-agarose resin (BioLog). After binding of the cAMP binding proteins, the resin was washed exhaustively with lysis buffer and the purified Bcy1 variants were unbound using elution buffer (20 mM MES, 40 mM cAMP, pH 6). Protein purity was assessed by 10% SDS-PAGE with Coomassie Blue staining. Glycerol was added up to 20%, and the samples were stored at −20 °C. Since the Bcy1 proteins obtained by this purification protocol are bound to cAMP, which absorbs at 280 nm, protein concentration was estimated using Coomassie Blue staining of the protein bands compared to aliquots of different concentrations of BSA, that were visualised in the same gel.

For the purification of Bcy1 1-50, *E. coli* BL21-CodonPlus (DE3)-RIPL cells carrying plasmid pET32a-Bcy1-50 were pelleted after overexpression of the recombinant fusion protein, and resuspended in lysis buffer (50 mM HEPES, 100 mM NaCl, 50 mM imidazole, pH 7) supplemented with protease inhibitor cocktail (Roche). Clarified whole cell lysates were obtained by disruption of the cell suspension with glass beads and further centrifugation for removal of the cellular debris. The lysate was incubated for 1 hour at 20 °C with Ni^{2+} HisLink resin (Promega) for binding of the fusion protein via the polyhistidine tag, and the resin washed exhaustively with lysis buffer. Removal of the tag was achieved by incubation of ~5 mg of the immobilised fusion protein with 5 U of enterokinase (Novagen) in enterokinase cleavage buffer (20 mM Tris–HCl, 50 mM NaCl, 2 mM $CaCl_2$, pH 7.4) for 16 h at 20 °C. The tag remained bound to the resin, whereas the partially purified Bcy1 1-50 was released to the supernatant, which was used for a SEC purification step (see size-exclusion chromatography below for details). Finally, to remove the small amount of contaminant proteins which eluted from the SEC in the same peak as Bcy1 1-50, an ion-exchange purification step was implemented. The protein eluted from SEC was concentrated using Vivaspin 500 concentrators (GE Healthcare) and incubated in batch with DEAE-cellulose (Sigma) previously equilibrated with HEPES 50 mM, pH 7, for 30 min at 20 °C. The supernatant containing the purified Bcy1 1-50 was recovered. Purity of the protein was assessed by 15% Tricine SDS-PAGE with silver staining. Aliquots were pooled and quantified by absorbance at 280 nm using a NanoDrop spectrophotometer, with the calculated molar absortivity of 1490 M^{-1} cm^{-1}. The identity of the purified fragment was assessed by MALDI-TOF-TOF mass spectrometry using a Bruker Ultraflex II spectrometer.

2.4. Sequence analysis

Amino acid sequences of PKA R subunits (Supplementary Table 1) were retrieved from the UniProtKB database (www.uniprot.org) using BLAST with mammalian proteins as the query sequences. Multiple sequence alignments of the whole collection were performed using Clustal Omega (McWilliam et al., 2013). Secondary structure predictions were performed using the PHYRE2 server (Kelley and Sternberg, 2009).

Sequence alignments of *Homo sapiens* RIα, (P10644), *H. sapiens* RIβ (P31321), *H. sapiens* RIIα (P13861), *H. sapiens* RIIβ (P31323), *Bos taurus* RIα, (P00514), *Rattus norvegicus* RIIα (P12368) and *S. cerevisiae* Bcy1 (P07278), were performed using the align2d command of the MODELLER package (Eswar et al., 2006), which considers structural information of the sequences for which a pdb file is available, and edited manually. For more accurate secondary structure predictions of Bcy1, four web servers that use different algorithms were used: PSIPRED (McGuffin et al., 2000), SCRATCH (Cheng et al., 2005), Jpred (Cole et al., 2008) and PredictProtein (Yachdav et al., 2014). The consensus secondary structure prediction was constructed considering the most frequently predicted secondary structure element for each amino acid.

Please cite this article in press as: González Bardeci, N., et al. The PKA regulatory subunit from yeast forms a homotetramer: Low-resolution structure of the N-terminal oligomerization domain. J. Struct. Biol. (2015), http://dx.doi.org/10.1016/j.jsb.2015.12.001

2.5. Chemical crosslinking experiments

Approximately 20 μg of Bcy1 WT, Bcy1 Δ1-85 or Bcy1 1-50 were diluted in 20 mM HEPES, 0.2 M KCl, 10 mM DTT and 1 mM EDTA, pH 7.5. A concentrated solution of the crosslinking reagent ethylene glycol bis[succinimidylsuccinate] (EGS) (Sigma) in DMSO was added to the protein dilution to a final concentration of the crosslinking reagent of 0.5–5.0 mM, and a DMSO concentration lower than 10%. The reaction proceeded for 30 min at room temperature in a final volume of 1 mL, and was stopped by the addition of Tris–HCl 50 mM, pH 9. The reaction products were precipitated with trichloroacetic acid, the pellets were washed exhaustively with cold acetone to remove excess-precipitating agent, and then were analysed by SDS-PAGE.

2.6. Size-exclusion chromatography

To perform the SEC purifications of Bcy1 1-50, a Superdex 75 GL 10/300 column (GE Healthcare) coupled to a Knauer Smartline Pump 1050 HPLC with a UV–Visible detector 2520 was used. The column was equilibrated with PBS buffer (20 mM phosphate, 150 mM NaCl, pH 7.4), and aliquots of 500 μL of partially purified protein were injected using an appropriate loop. The chromatography was developed at 20 °C at a flow rate of 1.0 mL/min under isocratic conditions, and the absorbance was monitored at 280 nm. Fractions containing the purified Bcy1 1-50 were pooled and concentrated using Vivaspin 500 concentrators (GE Healthcare).

To estimate the Stokes radius (R_s), the column was calibrated with protein markers of known Stokes radius: BSA (3.55 nm; 66.4 kDa), ovalbumin (2.80 nm; 45 kDa), α-chymotrypsin (2.09 nm; 25 kDa), and cytochrome C (1.70 nm; 12.3 kDa); all the standard proteins were from Sigma. A plot of $(-\log K_{av})^{1/2}$ vs R_s was built, where $K_{av} = (V_e - V_0)/(V_t - V_0)$ (V_e is the elution volume of the protein standard, V_0 and V_t are the void volume and the total volume of the column respectively; the V_0 was determined using Blue Dextran and the V_t was determined using acetone). For this determination, only a 100 μL aliquot of purified Bcy1 1-50 were injected into the column, to obtain better resolution.

To perform the SEC analysis of Bcy1 WT, a Superdex 200 GL 10/300 column (GE Healthcare) was used. The column was equilibrated with PBS buffer (20 mM phosphate, 150 mM NaCl, pH 7.4), and aliquots of 100 μL of purified protein were injected. The chromatography was developed at 20 °C at a flow rate of 0.6 mL/min under isocratic conditions, and the absorbance was monitored at 280 nm. The protein standards used were BSA (66.4 kDa) and aldolase (158 kDa) (Sigma).

2.7. Static light scattering measurements

The average molecular mass of Bcy1 1-50 and Bcy1 WT in solution was determined on a Precision Detectors PD2010 90° light scattering instrument connected in tandem with an HPLC and a LKB 2142 differential refractometer. The columns used were: Superdex 75 GL 10/300 for Bcy1 1-50, and Superdex 200 GL 10/300 for Bcy1 WT (GE Healthcare). A 100 μL sample of each purified protein was injected into the column, and the chromatographic runs were performed with PBS buffer (20 mM phosphate, 150 mM NaCl, pH 7.4) under isocratic conditions at a flow rate of 0.4 mL/min at 20 °C. The concentration of the injected samples was ~100 μM for Bcy1 1-50 and ~20 μM for Bcy1 WT. The molecular weight of each sample was calculated relating its 90° scattered light intensity and refractive index signals, and comparing this value with the one obtained for BSA (Mw: 66.5 kDa) as a standard using the software Discovery32.

2.8. Circular dichroism spectroscopy

CD spectra were recorded in the far UV (190–260 nm) using a Jasco J-815 spectropolarimeter equipped with a Peltier temperature control system, using a 1 mm path length quartz cell. A scanning speed of 50 nm/min and a spectral bandwidth of 2 nm were used. For each sample, 5 spectra were recorded and the results presented as the average spectrum to reduce background noise. Data were collected at 25 °C or 90 °C in PBS buffer (20 mM phosphate, 150 mM NaCl, pH 7.4). The protein concentration for CD spectroscopy was between 10 and 100 μM.

Thermal stability of the protein was measured by heating the samples at a rate of 2 °C/min and following the CD signal at 221 nm. The CD signals of the different samples were normalised and the melting temperature (T_m) was calculated by fitting the following equation to the normalised signal: CD $(T) = (\mathrm{IN} + \mathrm{bN}.T) + (\mathrm{IU} + \mathrm{bU} \times T)/(1 + \exp(-(T - T_m)/v))$, were T is the temperature, IN and IU are the normalised CD signals of the native and unfolded states at 0 °C respectively, bN and bU represent the thermal dependences of these signals, and v is a geometric factor that accounts for the cooperativity of the curves.

2.9. Sucrose gradient sedimentation

Sucrose gradient sedimentation experiments were performed using a Beckman Optima XL-90 ultracentrifuge with a SW 55 Ti swinging-bucket rotor. For each experiment, 200 μL of PBS buffer (20 mM phosphate, 150 mM NaCl, pH 7.4) containing catalase, BSA, ovalbumin, cytochrome c, and 100 μM Bcy1 1-50, were loaded onto a 5–20% sucrose gradient in PBS buffer. The rotor was operated for 18 hours at 4 °C and 100,000g. Fractions of 150 μL were collected from the bottom of the gradient and proteins in each fraction were analysed by 10% glycine SDS-PAGE and 15% tricine SDS-PAGE with Coomassie Blue staining.

2.10. Small angle X-ray scattering

SAXS data were collected using a SAXSess line collimation (10 mm) instrument (Anton Paar), using CuKα radiation (λ = 1.54 Å) and an image plate detector. After collection, the 2D data were reduced to $I(Q)$ vs Q, where $Q = (4\pi \sin\theta)/\lambda$ (2θ is the scattering angle and λ corresponds to the wavelength of the incident beam), using the program SAXSquant 2.0. For data collection, purified samples of Bcy1 1-50 were placed in a capillary cuvette at 12 °C in 25 mM HEPES buffer pH 7.0 and 50 mM NaCl. The X-ray scattering profile of the protein was obtained after buffer subtraction. Protein samples of ~2.8 mg/mL (500 μM) and ~5.8 mg/mL (1 mM) were studied to assess effects of protein concentration on I_0. Both Guinier plots were linear and the profile at the low Q region showed no aggregation effects; the forward scattered intensity (I_0) was proportional to the concentration of the sample. Therefore, we decided to work with the more concentrated sample, which presented better signal to noise ratio. The molecular mass of the protein was estimated as previously reported (Mylonas and Svergun, 2007) by comparison with a reference sample of lysozyme of know concentration.

The distance-distribution function of the particle, P(r), was obtained using the indirect Fourier transform method implemented in the program GNOM of the ATSAS software package (Svergun, 1992). The program also corrects the data for slit-smearing effects; for that purpose, the beam length profile parameters AH = 0.283 $Å^{-1}$ and LH = 0.181 $Å^{-1}$ were used. In addition, GNOM provides the I_0, the radius of gyration (R_g) and the maximum linear dimension (D_{max}) of the particle. The latter is provided by the user as a parameter for the calculation; the best value was the one that provided the better fit, and was chosen

Please cite this article in press as: González Bardeci, N., et al. The PKA regulatory subunit from yeast forms a homotetramer: Low-resolution structure of the N-terminal oligomerization domain. J. Struct. Biol. (2015), http://dx.doi.org/10.1016/j.jsb.2015.12.001

taking into consideration the statistical parameters provided by the program and the visual inspection of the $P(r)$ curve.

The *ab initio* SAXS models were generated using the program DAMMIF (Franke and Svergun, 2009) and further processed using the program suite DAMAVER (Volkov and Svergun, 2003) of the ATSAS software package. Twenty models were generated with DAMMIF from the $P(r)$ function calculated by GNOM, using the default parameters and imposing a P4 (tetramer) symmetry. DAMSEL was used to align the 20 models; one model which did not align well with the others was discarded. The remaining 19 models were averaged using DAMSUP and DAMAVER. For the average structure, DAMFILT was used to remove low occupancy regions and loosely connected atoms. All the DAMAVER programs were used with the default parameters and imposing a P4 symmetry.

2.11. Model construction

The homology model of the Bcy1 1-50 dimer was generated with the MODELLER package (Eswar et al., 2006), using a structural alignment of Bcy1 amino acids 1-50 with the apo RIIα D/D structures (pdb codes: 1R2A (NMR), 1L6E (NMR) and 2IZY (crystal)), generated with the command align2D implemented in the program. The sequence similarity between the target and the templates is ~38%. Twenty models were generated imposing symmetry restraints, and the best four models according to the DOPE score provided by MODELLER were refined using the KoBaMIN server (Rodrigues et al., 2012). The refined models were submitted to the QMEAN (Benkert et al., 2009) and PDBsum (de Beer et al., 2014) servers for quality assessment. The best model presented 92.4% of residues in the most favourable regions of Ramachandran plot, and no residue in the disallowed regions. The PROCHECK evaluation revealed no individual G-factor under −0.5 and an overall G-factor of 0.42 (the G-factor indicates the average quality of bond lengths and angles; for a model to be reliable, the G-factor should be above −0.5). The QMEAN score provides an estimate of the global reliability of a homology model; it is expected to be close to 1 for good models. The score for the best model was 0.836 which is very similar to that of the templates. Therefore, the resulting model was satisfactory from both global and local quality estimators.

To construct the model of the tetramer, the model of the dimer was used both as receptor and as ligand for docking using the ClusPro protein docking server (Comeau et al., 2004). The server generated 93 models which were further processed to select the best one as described in Section 3. The resulting model was analysed with PDBsum. It is important to mention that when different dimeric models were used as templates for ClusPro, similar results for the tetrameric model were obtained.

All the models were analysed and the images generated using Visual Molecular Dynamics (Humphrey et al., 1996).

3. Results

3.1. Bioinformatic analysis of the D/D domains from fungi

To get an insight into the structural features of the D/D domain of Bcy1, we first analysed the N-terminal region of fungal PKA R subunits to search for dimerization determinants. A phylogenetic study of the cAMP-binding domains has been reported previously (Canaves and Taylor, 2002), but the D/D domains have not been studied using this approach. To start, we generated a collection of 99 fungal sequences (Supplementary Table 1) and performed a multiple sequence alignment of the region preceding the IS (Supplementary Fig. S1). A first inspection of the alignment revealed that 36 fungal sequences lack the N-terminal region, corresponding to the canonical D/D domain. In agreement with this observation, secondary structure predictions performed on all the proteins of the collection showed that this group is lacking the characteristic N-terminal helix-turn-helix motif, but instead has an intrinsically disordered region (Supplementary Fig. S1). The other 63 fungal sequences do have a predicted helix-turn-helix motif. It is interesting to note that all the fungal species that lack a D/D domain according to the bioinformatic predictions belong to the pezizomycotina subphylum (Table 1). The R subunits from these species are therefore expected to be monomeric.

3.2. Mapping of the D/D domain of Bcy1

Bcy1 has been reported to be dimeric *in vitro* (Hixson and Krebs, 1980; Johnson et al., 1987). However, the region of the molecule responsible for dimerization has not been identified. The Pfam database (www.pfam.com) predicts that Bcy1 has the classic domain architecture of PKA R subunits (Fig. 1a). We therefore examined in more detail the N-terminal region, where the D/D domain is likely to occur, using secondary structure predictions and a multiple sequence alignment including mammalian R subunits with known structure.

The secondary structure prediction of Bcy1 indicates that residues 8-48 are likely to fold into a helix-turn-helix motif, as occurs in mammalian D/D domains (Fig. 1b). A remarkable characteristic of Bcy1 is that helix 2 is predicted to be five amino acids longer (one and a half helical turns) than that of mammalian proteins. The extension of helix 2 predicted for mammalian RII D/D domains is in agreement with the experimental one (data not shown), confirming the validity of the prediction for Bcy1.

Specific residues have been reported to disrupt dimerization of mammalian R subunits when mutated to alanine: in human RIIβ, Ala mutation of Leu^{13} or Phe^{36} prevents dimerization (Li and Rubin, 1995); in bovine RIα, Ala mutation of Phe^{47} or Phe^{52} also generates monomeric proteins (Banky et al., 1998). These residues and the central proline, which is the landmark residue of the loop separating both helices, are strictly conserved in Bcy1 (Fig. 1b).

Since the D/D domains of RI and RII share a similar fold, many of the residues involved in important dimer interactions are conserved among all types of R subunits; however, some differences exist. Therefore, to analyse the conservation of these residues in Bcy1, it was useful to compare it separately with RIα and RIIα. From the analysis, clear differences arise regarding the conservation of residues in Bcy1 (Fig. 1b): 71.4% of the residues that establish important interactions in the D/D domain structure of RIIα are either strictly conserved or conservatively substituted in Bcy1,

Table 1
Distribution of D/D domains across fungi.

Phylum	Subphylum	With D/D	Without D/D	Total
Ascomycota	Pezizomycotina	10	36	46
	Saccharomycotina	25	0	25
	Taphrinomycotina	2	0	2
Basidiomycota[a]	–	14	0	14
–	Mucoromycotina[b]	10	0	10[c]
Chytridiomycota		1	0	1
Blastocladiomycota		1	0	1
Total		63	36	99

[a] All fungi from the three subphylum of Basidiomycota (Pucciniomycotina, Ustilaginomycotina and Agaricomycotina) were found to have a predicted D/D domain.

[b] The subphylum Mucoromycotina belonged to the zigomycetes phylum, and now it is considered as a basal fungal lineage which diverged from the dikarya (ascomycetes and basidiomycetes) monophyletic group.

[c] The 10 sequences of Mucoromycotina come from only two organisms: *Mucor circinelloides* (4 sequences) and *Rhizopus delemar* (6 sequences).

Please cite this article in press as: González Bardeci, N., et al. The PKA regulatory subunit from yeast forms a homotetramer: Low-resolution structure of the N-terminal oligomerization domain. J. Struct. Biol. (2015), http://dx.doi.org/10.1016/j.jsb.2015.12.001

whereas only 37.5% of those residues fulfil this criteria when comparing Bcy1 with RIα. This observation, together with the α-helix topology of Bcy1 (which is more similar to RIIα than to RIα) and the lack of the cysteines that are involved in interchain disulfide bonds only in RIα (Fig. 1b), suggests that the Bcy1N-terminus may be classified as a "RIIα-like" D/D domain.

The conservation of residues essential for dimerization of mammalian R subunits in Bcy1 and the secondary structural elements organisation strongly suggest that the D/D domain of Bcy1 is located within the first 50 amino acids of the protein, and that the structural features associated with dimerization are similar to those of mammalian proteins.

To verify this prediction, we performed chemical crosslinking experiments to assess the oligomeric state of purified preparations of Bcy1 WT and Bcy1 Δ1-85. This deletion mutant lacking the putative D/D domain is of interest since, in contrast to full-length Bcy1, it is unable to bind partners such as Ira2 and Hsp60 (Galello et al., 2014). The homobifunctional reagent ethylene glycol bis[succinimidylsuccinate] (EGS) was used for crosslinking because it specifically crosslinks amino groups such as N-terminal or lysine ε-amino groups, allowing the capture of complexes which are sustained by non-covalent interactions. Several protein bands corresponding to oligomers of Bcy1 WT appeared in the SDS-PAGE of samples treated with EGS, including a very noticeable band with molecular mass corresponding to a dimer (Fig. 2); however, no additional bands appeared for Bcy1 Δ1-85 after treatment with EGS. These results demonstrate that the WT protein is capable of forming oligomers in solution, and that the oligomerization determinants are located within the first 85 amino acids of the protein, in accordance with the predictions from the sequence analysis.

3.3. Production of the D/D domain of Bcy1

Since residues 51-85 of Bcy1 are predicted to be unstructured according to secondary structure prediction algorithms (data not shown), the 1-50N-terminus of Bcy1 should be sufficient to represent the entire structure of the putative D/D domain. We therefore cloned and overexpressed this sequence in *E. coli* as a fusion protein which contains at its N-terminus a 158-amino acid tag consisting of a thioredoxin tag, a histidine tag, an S-tag, and an enterokinase cleavage site. Purification was achieved in four steps: binding to a Ni^{2+} resin, on-column treatment of the immobilised fusion protein with enterokinase (which releases the fragment Bcy1 1-50 with an additional alanine residue at the N terminus), size-exclusion chromatography (SEC) purification of the released cleavage product and finally incubation of the Bcy1 1-50 containing fractions with DEAE-cellulose for removal of the remaining impurities. The protein was obtained with high purity (Fig. 3a), and its identity was assessed by MALDI-TOF mass spectrometry (data not shown), confirming that a fragment with the expected molecular mass of 5.9 kDa was produced.

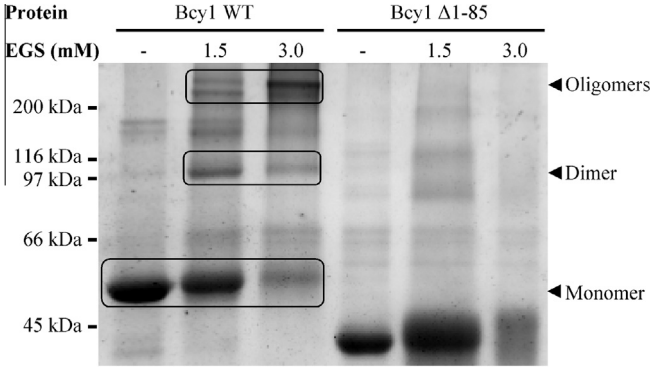

Fig. 2. Mapping of the D/D domain of Bcy1. Purified samples of Bcy1 WT and Bcy1 Δ1-85 were treated with the crosslinking reagent EGS, analysed by 10% SDS-PAGE and the reaction products visualised by Coomassie Blue staining. The expected molecular masses of the different forms are 47 kDa (monomer) and 94 kDa (dimer).

The purified protein fragment eluted from the SEC column as a single peak with an elution volume slightly higher than that of α-chymotrypsin; therefore, its apparent molecular mass in solution is ~25 kDa (Fig. 3b). It is possible that this unexpected behaviour (the expected molecular mass for a dimer is 11.8 kDa) is a consequence of an elongated, non-spherical shape; however, since mammalian D/D domains are highly compact, it is also possible that a higher order association exists. Because a higher order oligomer structure would be unique among the D/D domains described to date, we proceeded to study in detail the oligomeric state of Bcy1 1-50 in solution.

3.4. Oligomeric state of Bcy1 1-50 in solution

The ability of Bcy1 1-50 to form oligomers was first evaluated by chemical crosslinking of the purified protein with EGS. Several bands corresponding to dimer, trimer and tetramer appeared on SDS-PAGE after treatment with EGS (Fig. 3c). This result suggests that, unexpectedly, Bcy1 1-50 could form oligomeric structures containing up to 4 subunits.

Since the expected molecular mass for a tetramer is 23.6 kDa, the existence of a tetrameric structure could explain the anomalous behaviour observed in the SEC profile (Fig. 3b); the fact that a single peak was observed by SEC suggests that this oligomeric state is the predominant species in solution. However, it is not possible to discard the possibility that multiple oligomeric forms coexist; in fact, after rerunning the eluted SEC peak fractions, a peak shift to higher volume (i.e., lower molecular mass) was observed (data not shown), suggesting that the different oligomeric forms may coexist in rapid exchanging equilibrium. However, it should be noted that the presence of dimer and trimer complexes in the chemical crosslinking experiments does not necessarily indicate that these structures exist in solution, since in such experiments it is usual to observe the intermediate forms owing to inefficient crosslinking of multi-subunit complexes.

To further explore the oligomeric structure of Bcy1 1-50, we performed SEC-coupled static light scattering (SLS) measurements on a purified sample of Bcy1 1-50 at 100 μM (Fig. 3d). The average molecular mass of the single eluted peak was (23.5 ± 0.7) kDa, which is in excellent agreement with the expected molecular mass for the tetramer (23.56 kDa). This result confirms that under these experimental conditions Bcy1 1-50 exists in solution as a single species which consists of four subunits.

3.5. Oligomeric state of Bcy1 WT in solution

Since tetrameric structures have not been reported for D/D domains of any source, we considered the possibility that the previous results were an artefact owing to either the protein fragment or the expression system we used. However, it is worth noting that previous structural studies of mammalian D/D domains have been performed using a similar recombinant construct expressed in bacteria. We performed SEC-SLS using a 20 μM sample of full-length Bcy1 WT purified from yeast to evaluate the existence of a previously unreported tetrameric species. This technique has not been used previously to assess the molecular mass of Bcy1 in solution. The protein eluted from the SEC column as a single peak with an average molecular mass of (230 ± 20) kDa (Fig. 4a). Since the molecular mass of Bcy1 is 47.2 kDa, the number of subunits determined from the SLS experiment is (4.9 ± 0.4); therefore, under these conditions, Bcy1 is either tetrameric or pentameric in solution. The existence of a pentameric species would be inconsistent with the results for Bcy1 1-50 showing a tetrameric structure. The difference in

Please cite this article in press as: González Bardeci, N., et al. The PKA regulatory subunit from yeast forms a homotetramer: Low-resolution structure of the N-terminal oligomerization domain. J. Struct. Biol. (2015), http://dx.doi.org/10.1016/j.jsb.2015.12.001

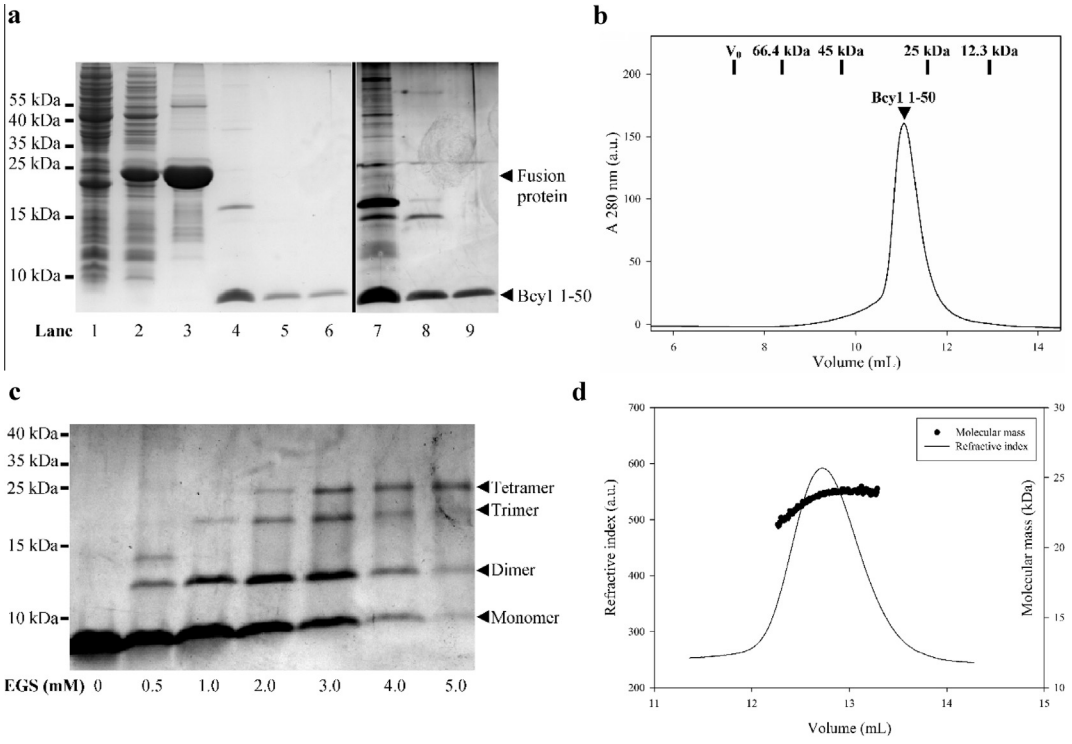

Fig. 3. Purification and oligomeric state of Bcy1 1-50 in solution. (a) Fractions from the different steps of the purification were analysed by 15% Tricine SDS-PAGE and visualised by Coomassie Blue staining. 1: clarified whole cell lysate from a non-induced culture of an *E. coli* strain which expresses the recombinant fusion protein. 2: whole cell lysate from the same strain upon IPTG induction. 3: Ni^{2+} resin after binding of the fusion protein and washing. 4: supernatant of enterokinase treatment of the immobilised fusion protein; the tag is retained in the resin. 5: peak corresponding to Bcy1 1-50 from SEC using a Superdex 75 column. 6: supernatant of the batch incubation of the SEC eluate with DEAE-cellulose. 7, 8 and 9 are the same as 4, 5 and 6, visualised with silver staining. The 22.9 kDa band corresponds to the fusion protein whereas the 5.9 kDa band corresponds to Bcy1 1-50. (b) SEC elution profile of a 100 μM sample of Bcy1 1-50 performed at 25 °C in PBS buffer in a Superdex 75 column. The concentration was detected as the absorbance at 280 nm. (c) Purified samples of Bcy1 1-50 were treated with EGS, analysed by 15% Tricine SDS-PAGE and visualised by Coomassie Blue staining. The molecular masses of the different forms are: 5.9 kDa (monomer), 11.8 kDa (dimer), 17.7 kDa (trimer), and 23.6 kDa (tetramer). (d) SEC-coupled SLS measurements of a purified 100 μM sample of Bcy1 1-50 were performed at room temperature in PBS buffer. The concentration was detected as a function of the refractive index signal. The average molecular mass, calculated from the 90° scattered light intensity, was (23.5 ± 0.7) kDa.

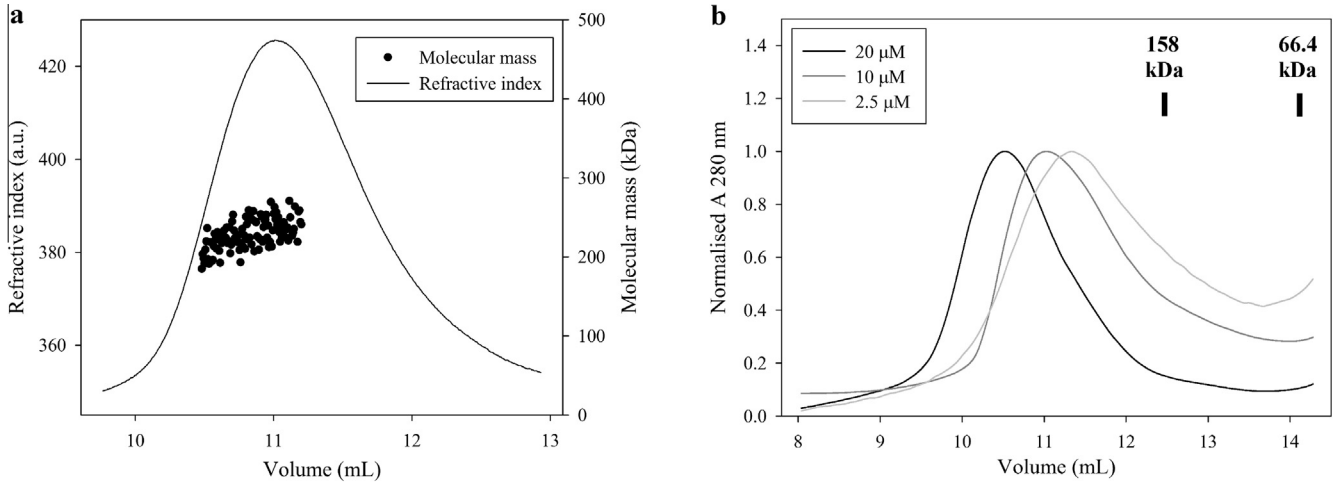

Fig. 4. Oligomeric state of Bcy1 WT in solution. (a) SEC-coupled SLS measurements of a purified 20 μM sample of Bcy1 WT were performed at room temperature in PBS buffer. The concentration was detected as a function of the refractive index signal. The average molecular mass, calculated from the 90° scattered light intensity, was (230 ± 20) kDa. (b) SEC elution profile of purified samples of different concentrations of Bcy1 WT was performed at 25 °C in PBS buffer in a Superdex 200 column. The concentration was detected as the absorbance at 280 nm. The spectra were normalised for comparison.

apparent oligomeric structures is more likely due to difficulties in estimating the molecular mass of Bcy1 due to lower signal no noise ratio in these SEC-SLS experiments. A lower concentration of the Bcy1 WT sample (20 μM) compared to that of Bcy1 1-50 (100 μM) was used, and the chromatographic of the Bcy1 WT samples presented much higher background noise. In support of the SEC-SLS results of Bcy1 WT, protein bands of ~200 kDa were observed in the chemical crosslinking experiments (Fig. 2).

These results are in disagreement with the previous reports of dimeric structures for Bcy1 (Hixson and Krebs, 1980; Johnson et al., 1987). To evaluate the presence of dimeric Bcy1 in our preparations, we performed SEC of purified samples of Bcy1 at different

Please cite this article in press as: González Bardeci, N., et al. The PKA regulatory subunit from yeast forms a homotetramer: Low-resolution structure of the N-terminal oligomerization domain. J. Struct. Biol. (2015), http://dx.doi.org/10.1016/j.jsb.2015.12.001

concentrations. The protein eluted as a single peak with an apparent molecular mass higher than 158 kDa at all the concentrations tested, which is consistent with the existence of the 190 kDa-tetramer (Fig. 4b). However, the peak of the more concentrated sample shifted to higher elution volumes (i.e., lower molecular masses) after dilution. This observation suggests that the tetramer coexists with lower-molecular mass forms in a rapid exchanging equilibrium and, as expected for an oligomerization process, this equilibrium is concentration-dependent.

Taken together, these and the previous section's results strongly support the idea that a tetrameric form of Bcy1 exists, and that its oligomerization is a dynamic process which occurs through its D/D domain. In the following sections we describe the structural characterization of the tetrameric Bcy1 1-50.

3.6. Secondary structure of Bcy1 1-50 in solution

The bioinformatic analysis predicted a helix-turn-helix motif for Bcy1 1-50 (Fig. 1b). To verify this prediction, secondary structure was evaluated using circular dichroism (CD) spectroscopy. The far-UV spectrum of a 12.7 μM sample of purified Bcy1 1-50 at room temperature has two sharp minima at 210 and 222 nm, which is typical of proteins with a high α-helical content (Fig. 5a). Samples ranging from 1.6 μM to 100 μM displayed very similar CD spectra, indicating that the secondary structure content of this protein is not dependent on concentration within this range (data not shown).

To study the thermal stability of the structure of this domain, CD spectra were recorded at 90 °C and at room temperature following incubation at 90 °C (Fig. 5a). After denaturation, full secondary structure recovery was achieved almost immediately. This observation proves that the thermal denaturation process is reversible for this domain, which provides evidence for the high stability of its fold. Thermal unfolding followed by CD recording at 221 nm displayed a cooperative behaviour that indicates a well packed structure (Fig. 5b). The melting temperature strongly depends on the total protein concentration, shifting from 50.4 °C for a 13 μM sample to 54.7 °C for a 63 μM sample; this behaviour is typical of oligomeric proteins.

3.7. Hydrodynamic properties of Bcy1 1-50

Next we determined characteristic hydrodynamic parameters of Bcy1 1-50 which are representative of the behaviour of the protein in solution: the Stokes radius (R_s), the sedimentation coefficient (s), the radius of gyration (R_g), and the maximum intraparticle distance (D_{max}).

The R_s of Bcy1 1-50 was calculated from the calibration of the SEC profile of Fig. 3b, which corresponds to a 100 μM sample; the value obtained was 2.3 nm (Supplementary Fig. S2). The sedimentation coefficient was estimated using sedimentation in a sucrose gradient with protein standards, using a 100 μM sample of Bcy1 1-50; the value obtained was 2.4 S (Supplementary Fig. S3). The combination of these hydrodynamic parameters allows the estimation of the molecular mass of the protein using the method of Siegel and Monty (1966). The value was 22.6 kDa, which corresponds to the molecular mass of a tetramer with an error of ~4%, in agreement with the SLS data. The frictional ratio f/f_0 was calculated to be 1.24, which is typical of globular proteins (Erickson, 2009).

To complete the hydrodynamic characterization of Bcy1 1-50, we performed small-angle X-ray scattering (SAXS) experiments. This technique provides low-resolution structural information (size and overall shape) of macromolecules in solution (Mertens and Svergun, 2010). Because the intensity of X-ray scattering of a protein is proportional to its concentration and to the square of its molecular mass, a sample of high concentration was required to obtain good quality SAXS data; therefore, a 1.0 mM sample of purified Bcy1 1-50 was used (ten-fold higher than that of the SEC and SLS experiments). The shape of the scattering profile in the low Q region (Fig. 6a) and the linearity of the Guinier plot (Fig. 6b) indicated that the samples were monodisperse, without evidence of aggregation. The I_0 was proportional to protein concentration with a 2-fold dilution of the protein, indicating the lack of interparticle effects at the concentration of protein used for these studies (data not shown).

The $P(r)$ curve (Fig. 6c), which provides information regarding distances between every pair of atoms within a particle, was computed from the scattering profile by the indirect Fourier transform method implemented in the program GNOM (Svergun, 1992). The function is bell-shaped, with no distinct features, indicating that this is a relatively compact, globular protein. The R_g was 1.83 nm as calculated from the best fit obtained for the $P(r)$ function (this value is typically considered to be more accurate than the one provided by the Guinier approximation). The D_{max} (the value where the $P(r)$ curve drops to zero in Fig. 6c) was 5.5 nm. The ratio R_g/R_s is 0.82, which is also typical of globular proteins (Receveur-Brechot and Durand,

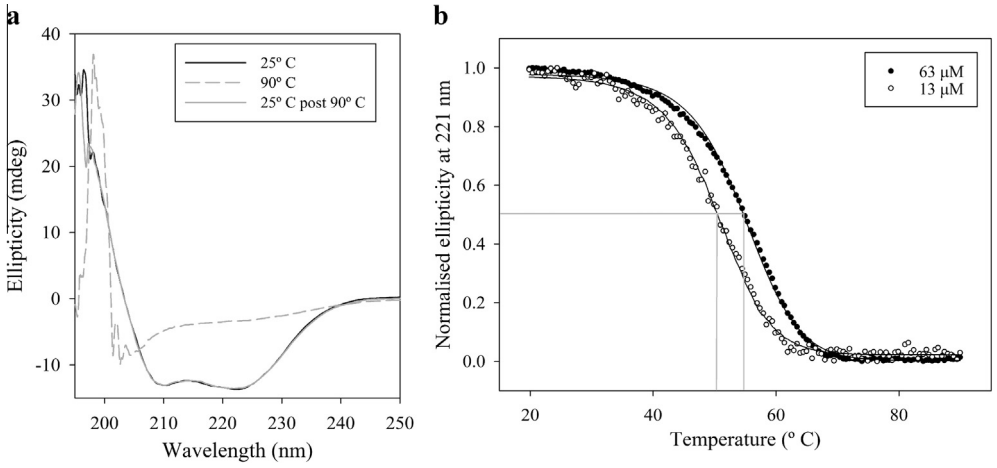

Fig. 5. CD spectroscopy of Bcy1 1-50. (a) Far-UV CD spectra of a 12.7 μM sample of purified Bcy1 1-50 were recorded in PBS at three different conditions: native, 25 °C (solid black line); unfolded, 90 °C (grey split line) and refolded at 25 °C after denaturation at 90 °C (grey solid line). (b) Thermal unfolding of two samples of different concentrations of Bcy1 1-50 was monitored by ellipticity at 221 nm in PBS. The experimental data are indicated in dots, and the fit corresponding to a two state transition model is shown in solid black lines. The gray lines indicate the melting temperatures of the two samples extrapolated from the theoretical curves.

Please cite this article in press as: González Bardeci, N., et al. The PKA regulatory subunit from yeast forms a homotetramer: Low-resolution structure of the N-terminal oligomerization domain. J. Struct. Biol. (2015), http://dx.doi.org/10.1016/j.jsb.2015.12.001

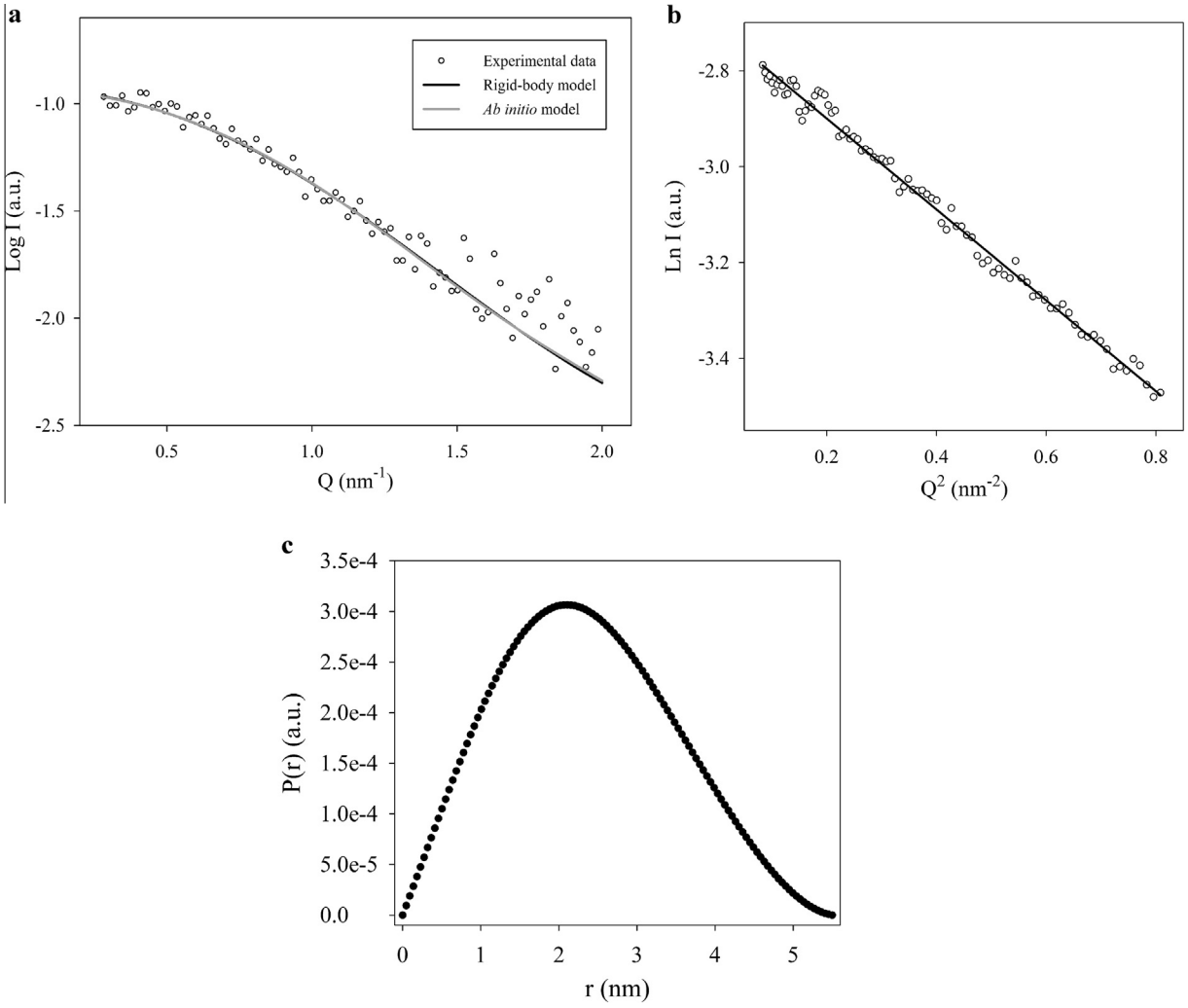

Fig. 6. SAXS characterization of Bcy1 1-50. SAXS data were collected using a 1 mM purified sample of Bcy1 1-50 at 12 °C in 25 mM HEPES buffer, pH 7, with 50 mM NaCl. After appropriate blank subtraction, the data were processed to obtain (a) the experimental SAXS profile (white dots), (b) the Guinier plot, and (c) the distance-distribution function, $P(r)$. $Q = 4\pi \sin(\theta)/\lambda$ is the scattering vector, and I is the scattered intensity. The white dots in the Guinier plot represent the experimental data, whereas the black line represents the linear fit ($R^2 = 0.99$). The theoretical SAXS profiles of the average *ab initio* model and of the best rigid-body model both fit well the experimental data (a) according to the χ criterion provided by the FoXS server (1.83 for both models).

2012). The SAXS data-collection and scattering-derived parameters are summarized in Table 2.

Finally, we compared the hydrodynamic properties of Bcy1 1-50 with those of its mammalian counterparts. Although many high-resolution structures are available for the latter, no hydrodynamic characterization has been reported. Therefore, we used the program HYDROPRO (Garcia De La Torre et al., 2000) to compute the parameters of RIIα D/D domain from the pdb files (Table 3). This protein was selected for the comparison because of its higher sequence and structure similarity with Bcy1 1-50 (Fig. 1b). The values of all the properties of mammalian RIIα D/D domain are smaller than the ones of Bcy1 1-50, which is consistent with the former being a dimer and the latter a tetramer.

3.8. Model of the tetrameric Bcy1 1-50 in solution

To better understand the architecture of the tetrameric oligomer we constructed a variety of models of the Bcy1 1-50 tetramer using the available experimental information.

As a first approach, we generated *ab initio* shape models from the SAXS data. For this purpose, the $P(r)$ function of Fig. 6c was used as input for the program DAMMIF (Franke and Svergun, 2009), using the default parameters and imposing a P4 (tetramer) symmetry. 20 models were generated and further processed and analysed using the program DAMAVER (Volkov and Svergun, 2003). From this analysis one of the models was discarded because it was significantly different from the others. The remaining 19 models were averaged; the predicted SAXS profile of the average *ab initio* model fits well the experimental data (Fig. 6a).

We next constructed a rigid-body model of the tetramer using homology modelling and computer-aided protein docking methods. We reasoned that since most of the characteristic elements of the dimeric mammalian D/D domains are also present in Bcy1 1-50 (see Section 3.2), it is likely that the structure of the classical dimeric D/D domain is present in the tetramer, i.e., the tetramer may be regarded as a dimer of dimers. Therefore, the strategy consisted in first building a homology model of a Bcy1 1-50 dimer, and then to use this model as a template to generate a model of the tetramer by using docking methods.

The model of the dimer (Fig. 7) was generated with MODELLER (Eswar et al., 2006), using as templates the RIIα D/D domain solution and crystal structures, and refined using the KoBaMIN server (Rodrigues et al., 2012). The distribution of secondary structure elements in the model is in excellent agreement with the results

Please cite this article in press as: González Bardeci, N., et al. The PKA regulatory subunit from yeast forms a homotetramer: Low-resolution structure of the N-terminal oligomerization domain. J. Struct. Biol. (2015), http://dx.doi.org/10.1016/j.jsb.2015.12.001

Table 2
SAXS data-collection and scattering-derived parameters.

Data-collection parameters	
Instrument	SAXSess (Anton Paar)
Beam geometry	10 mm slit
Wavelength (Å)	1.54
Q range (nm^{-1})	0.2–2.0
Exposure time (min)	60
Concentration (mg/mL)	5.8–2.8
Temperature (°C)	12
Structural parameters[a]	
I_0 (cm^{-1}) [from P(r)]	0.119 ± 0.001
R_g (nm) [from P(r)]	1.83 ± 0.01
I_0 (cm^{-1}) [from Guinier]	0.121 ± 0.001
R_g (nm) [from Guinier]	1.76 ± 0.03
D_{max} (nm)	5.5 ± 0.3
Molecular mass determination[a]	
I_0 reference sample (cm^{-1})	0.090 ± 0.001
Concentration reference sample (mg/mL)	9.8
Molecular mass reference protein (kDa)	14.3
Estimated molecular mass Bcy1 1-50 (kDa)	21.4 ± 0.6
Molecular mass Bcy1 1-50 monomer (kDa)	5.9
Software employed	
Primary data reduction	SAXSquant 2.0
Data processing	PRIMUS/GNOM
Ab initio analysis	DAMMIF
Validation and averaging	DAMAVER
Rigid-body modelling	ClusPro/FoXS
Computation of model intensities	FoXS
Three-dimensional graphics representations	VMD

[a] The structural parameters and molecular mass are reported for the 5.8 mg/mL sample. The molecular mass was estimated by comparison with a reference sample of known concentration of lysozyme.

Table 3
Hydrodynamic properties of D/D domains.

Protein	MM (kDa)	s (S)	R_s (nm)	R_g (nm)
Bcy1 1-50	23.2 (23.5)[a]	2.4 ± 0.2[b]	2.3 ± 0.1[c]	1.83 ± 0.01[d]
RIIα D/D domain	10.8[e]	1.31 ± 0.02[f]	2.16 ± 0.04[f]	1.63 ± 0.04[f]
Bcy1 1-50 dimer model	11.8[e]	1.46[g]	2.09[g]	1.58[g]
Bcy1 1-50 tetramer model	23.6[e]	2.37 ± 0.01[h]	2.58 ± 0.02[h]	(1.84 ± 0.02)[h]

[a] The experimental molecular mass of Bcy1 1-50 was calculated using the Siegel and Monty formula. The value in parentheses indicates the result determined by SLS.

[b] s for Bcy1 1-50 was determined by sucrose gradient ultracentrifugation, and expressed as the average of three independent experiments with standard deviation.

[c] R_s for Bcy1 1-50 was determined by SEC, and expressed as the average of three independent experiments with standard deviation.

[d] R_g for Bcy1 1-50 was determined by SAXS. The error was obtained from the GNOM fit.

[e] The theoretical molecular masses of Bcy1 1-50 and RIIα D/D domains were determined from the aminoacid sequence.

[f] s, R_s and R_g for the high resolution, solution structure of RIIα D/D domain were calculated for each independent model in the pdb file (1R2A) using the program HYDROPRO with the default parameters, and the result presented as the average of all the models with standard deviation.

[g] s, R_s, and R_g for the dimer model of Bcy1 1-50 were calculated using the program HYDROPRO with the default parameters.

[h] s and R_s for the tetramer model of Bcy1 1-50 were calculated for each of the 5 better models that presented a similar topology using the program HYDROPRO with the default parameters, and the result presented as the average of all the models with standard deviation. The R_g was calculated with the values provided by FoXS.

of the secondary structure predictions. The model shows a well-defined core of hydrophobic residues, similar to RIIα, which is enriched in aromatic residues. The main difference, as discussed in Section 3.2, occurs at the end of helix 2, where an additional α-helical turn was modelled into Bcy1 1-50.

To generate the model of the tetramer, we used the automated docking server ClusPro (Comeau et al., 2004). This program generates, for a receptor and a ligand, several models of the complex which are further classified in terms of the main forces that sustain it (balanced, electrostatic-favoured, hydrophobic-favoured, and Van der Waals/electrostatic). The model of the Bcy1 1-50 dimer was used both as receptor and as ligand.

The server generated 93 models which displayed a great diversity of structures resulting from different orientations of the dimers. From these models, we reasoned that the ones which better agree with the SAXS results may be regarded as the most representative of the real structure in solution. Therefore, a selection protocol was performed as follows: all the models were submitted to the FoXS server (Schneidman-Duhovny et al., 2010), which allows for rapid comparison of theoretical SAXS profiles calculated from pdb files with experimental data; the server also provides an estimate of the R_g of the structure in the pdb file. R_g values ranged between 1.79 nm and 2.27 nm; abnormally high values were observed for several models due to imperfect packing of the dimers or to relative orientations that resulted in overly extended structures. Since the lowest R_g observed was 1.79 nm (0.04 nm lower than the experimental value) we set an upper limit of 1.87 nm (0.04 nm higher than the experimental value) and discarded the 60 models with R_g higher than the cut off. From the remaining 33 models, the 11 models that fit better the experimental SAXS data ($\chi < 1.9$ according to FoXS) were considered (Supplementary Table 2). These models (available as pdb files as Supplementary Material online) are clustered in ClusPro categories as follows: 1 model "balanced", 2 models "electrostatic", 7 models "electrostatic + Van der Waals" and 1 model "hydrophobic". From the 7 models of the third category, 5 models displayed very similar architectures regarding relative orientation of the dimers (Supplementary Table 2). The other observed folds were largely underrepresented among the best-ranked models. Therefore, we concluded that this fold is probably the most representative of the real structure in solution, and selected from these 5 models the one that fit better the experimental SAXS profile (Fig. 6a) for further analysis. This model is also the one that fits better the data from the 33 models that were not discarded for their R_g.

These models superimpose very well with the *ab initio* SAXS model (Fig. 8c), where each lobe represents one Bcy1 1-50 dimer. HYDROPRO (Garcia De La Torre et al., 2000) was used to calculate the hydrodynamic properties of the Bcy1 1-50 rigid-body models using their respective pdb files (Table 3). The predicted sedimentation coefficient for the tetramer models is in excellent agreement with the experimental value, whereas the predicted R_s is higher. These differences in R_s values calculated by HYDROPRO may arise as a consequence of the treatment of the hydration layer (Schneidman-Duhovny et al., 2012). The R_g obtained with FoXS is in excellent agreement with the experimental value (1.84 and 1.83 nm, respectively).

Although it is not possible to obtain atomic level structural details from these models, several important structural features are apparent. First, the tetramer is sustained by the interaction of the solvent-exposed face of helix 2 of the four protein chains, and the dimers are packed in an antiparallel fashion with a symmetrical arrangement (i.e., the N-terminus of helix 2 of one chain of one of the dimers is packed against the C-terminus of helix 2 of one of the chains of the other dimer). Moreover, as predicted by the ClusPro server, there are many charged and polar residues clustered at the centre of this four-helix core; this is in contrast with the hydrophobic core that sustains the dimers themselves. The models support the idea of a tetrameric Bcy1 in which the D/D core lies at the centre of the structure, and the linkers of the four subunits extend radially from the C-terminus of each chain (Fig. 8b). It is interesting to note that in these models the two

Please cite this article in press as: González Bardeci, N., et al. The PKA regulatory subunit from yeast forms a homotetramer: Low-resolution structure of the N-terminal oligomerization domain. J. Struct. Biol. (2015), http://dx.doi.org/10.1016/j.jsb.2015.12.001

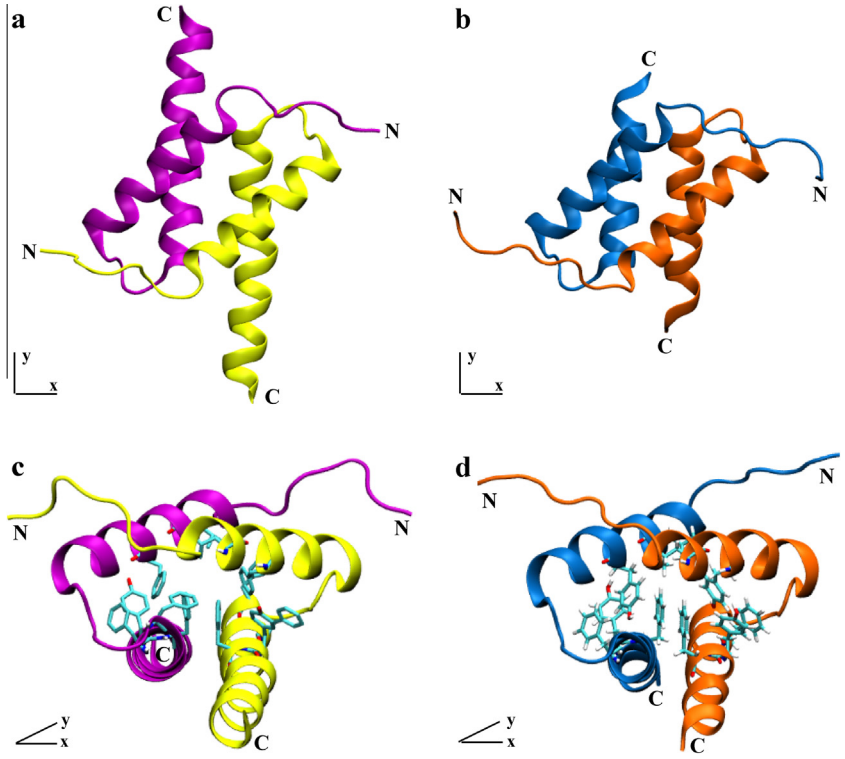

Fig. 7. Structure of dimeric D/D domains. The structure of the homology model of the Bcy1 1-50 dimer (a and c) and the NMR structure of RIIα D/D domain (pdb: 1R2A) (b and d) are shown in ribbon diagrams. The chains are represented in different colours for clarity purposes (Bcy1: yellow and purple, RIIα: orange and blue) and the N and C termini are indicated. The top panels show a view of the AKAP binding surface; the bottom views are rotated 90° across the *x*-axis. The main hydrophobic residues that constitute the dimerization core are indicated as sticks in the lower panels.

putative AKAP-binding surfaces remain exposed to the solvent, with their faces pointing to opposite sides of the complex. As a consequence of the tetrameric nature of this complex, the two AKAP-binding surfaces are retained, and new solvent-exposed surfaces are formed at the sites where the dimers contact.

4. Discussion

In this work, we present the first structural characterization of a non-mammalian PKA D/D domain. Using bioinformatic approaches, we found that the hydrophobic residues that constitute the core of dimerization and the secondary structure elements of mammalian D/D domains are well conserved in Bcy1. Furthermore the analysis indicates that, despite some characteristics which are typical of RIIα D/D domains, Bcy1 has unique features of its own, such as the extended helix 2. This is in agreement with the previously reported structure of the cAMP binding domains of Bcy1, which were also found to be different from both RIα and RIIα (Rinaldi et al., 2010).

Most R subunits are typically regarded as being dimers. However the bioinformatic analysis of fungal PKA sequences revealed that a group of fungi lack the D/D domain (Supplementary Fig. S1). Since monomeric R subunits with no D/D domain have already been reported in some organisms like *Paramecium* (Carlson and Nelson, 1996) and *Dictyostelium* (de Gunzburg and Veron, 1982; Mutzel et al., 1987), the lack of a D/D domain predicts a monomeric form for those fungal R subunits. However, some discrepancies from this prediction exist: the R subunit of *Neurospora crassa*, which we have found to lack a D/D domain, has been reported to be dimeric (Trevillyan and Pall, 1982) and the R subunit of *Yarrowia lypolitica*, which contains the sequence of a canonical D/D domain with an additional ~20 amino acid sequence at the N-terminus, has been shown to be monomeric (Kronberg et al., 2011).

Regarding the quaternary structure of Bcy1 D/D domain an unexpected result was obtained since, unlike the well-established dimeric structure of mammalian D/D domains, it is a tetramer in solution. This may be the result of slight differences at the C-terminus of the D/D domain: the construct Bcy1 1-50 presents one and a half additional turns at the end of helix 2, and also some differences in the amino acid composition; a gap had to be introduced in order to optimise the alignment in this region. We have also shown by SLS experiments the existence of a novel unreported tetrameric form for the full length Bcy1, consistent with the chemical crosslinking experiments that revealed high molecular mass forms. Moreover, the quaternary structure of Bcy1 seems to be dynamic in a concentration-dependent fashion, since the SEC peak shifts to higher volumes (i.e., smaller sizes) after dilution. Consistently, the same behaviour was observed for the D/D domain alone (data not shown). It has been reported that transient associations between proteins are dominated by polar interactions, in contrast to stable associations that are typically hydrophobic (Jones, 2012). In agreement with this observation, the model of the tetramer that we propose, derived from *ab initio* modelling from SAXS data and from rigid-body modelling, is sustained by electrostatic interactions between the helices 2 of the four protomers, in contrast with the interactions within each of the D/D domain dimers, which are mainly hydrophobic.

Besides binding to AKAPs, few PKA features require dimerization of the R subunit (see (Boettcher et al., 2011) for an example). Functional dimeric RC holoenzymes have been described (Carlson and Nelson, 1996; de Gunzburg and Veron, 1982; Mutzel et al., 1987; Paveto et al., 1989) suggesting dimerization is strongly related to interaction with partners. In fact, in the case of *S. cerevisiae*, the recently described interaction of Bcy1 with

Please cite this article in press as: González Bardeci, N., et al. The PKA regulatory subunit from yeast forms a homotetramer: Low-resolution structure of the N-terminal oligomerization domain. J. Struct. Biol. (2015), http://dx.doi.org/10.1016/j.jsb.2015.12.001

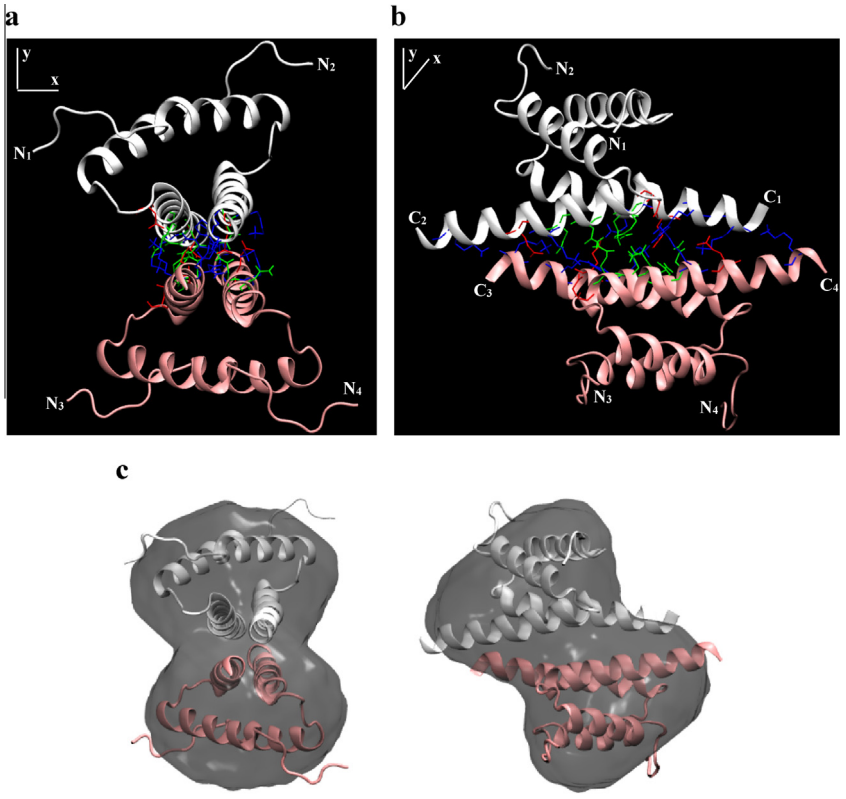

Fig. 8. Rigid-body model of the Bcy1 1-50 tetramer and comparison with the shape model. (a and b) Two views of the model of the tetrameric Bcy1 1-50 are shown in ribbon diagrams. The two dimers that constitute the tetramer are coloured pink and white, and the N and C termini are indicated, with the numbering of each protein chain in subscripts. The polar and charged residues that lie at the tetramer interface are shown as sticks in green (polar, uncharged), red (acidic) or blue (basic). The left panel emphasises the overall topology of the tetramer and the arrangement of the four helix 2 structures that constitute the core of tetramerization. The right panel is rotated 90° across the *y*-axis to show more clearly the characteristics of the amino acids at the interface. (c) The best superimposition of the rigid-body model with the shape model generated *ab initio* from the SAXS data was performed using SUPCOMB (Kozin and Svergun, 2001).

specific partners is dependent on the N-terminal 1-85 amino acids, and therefore on the 1-50 D/D domain characterised in this work. Matthews and Sunde discussed the origins and implications of oligomerization in biology (Matthews and Sunde, 2012). They proposed that organisms have evolved to maintain oligomerization because of functional advantages. For example, the localization of a binding site at a complex interface provides a mechanism of regulation through concentration-dependent oligomerization: when the concentration is sufficient to form the oligomer the binding site exists, whereas at lower concentrations the oligomer separates into its composing parts which do not exhibit such a surface. Another possible advantage is that the conformation of homo-oligomers could increase the number of interacting partners.

In our model of the tetrameric structure, two putative "classical" AKAP binding surfaces are preserved, which are predominantly hydrophobic binding sites, similar to mammalian D/D domains. However, the interactions with the recently reported Bcy1 partners are ruled by different determinants than those of classical mammalian D/D with AKAPs, which are dominated by non-polar residues. In Bcy1 interacting proteins, positive amino acids within the amphipathic α-helical interacting peptides are crucial for the interaction (Galello et al., 2014). In the tetramer model, new surfaces appear on both sides of the tetramer complex, which might provide novel interaction sites. Moreover, several negatively charged residues are solvent-exposed at these surfaces; therefore, it is possible that the reported partners do not interact with Bcy1 through the classical AKAP binding sites, but through these additional surfaces. This hypothesis would explain the differences in the properties of the amino acids in binding partners required to establish interactions with Bcy1.

A report was published during the preparation of this manuscript, identifying R and C subunits of PKA during eukaryotic evolution, including the presence or absence of a D/D domain in the R subunits (Peng et al., 2015). The existence or not of paralogues of known mammalian AKAPs is described as well as the detection of new putative AKAPs through cAMP-agarose pull down followed by mass spectrometry. An important group of fungi without a D/D domain is not described as such in this work, nor differences in the alignment of Bcy1 D/D domain with its mammalian partners. From an evolutionary and historic perspective, fungi are described as having developed a D/D domain but not the corresponding anchoring proteins that interact with those domains. However we favour the idea that, at least in *S. cerevisiae*, there are proteins interacting with Bcy1 D/D domain, although through different structural determinants than those of mammalian R subunits with AKAPs.

5. Conclusions

Here we report the first structural study of a non-mammalian PKA D/D domain. Surprisingly, we found that the D/D domain of Bcy1 is tetrameric in solution, and also discovered a novel tetrameric form of the full length Bcy1. The dynamism of the quaternary structure of Bcy1, together with the idea that its oligomerization state is related to interaction with partners, suggests a possible regulatory role for its oligomerization. While it remains to be studied if this structure exists *in vivo* as well as in other organisms, the evidence we present here strongly suggest that, unlike it was previously thought, a great diversity of oligomeric

Please cite this article in press as: González Bardeci, N., et al. The PKA regulatory subunit from yeast forms a homotetramer: Low-resolution structure of the N-terminal oligomerization domain. J. Struct. Biol. (2015), http://dx.doi.org/10.1016/j.jsb.2015.12.001

states exists for the R subunits of PKA. Further studies of *in vivo* oligomerization and high-resolution structure elucidation of the D/D domain of Bcy1 as well as D/D domains from other sources will also shed light on this topic.

Funding

This work was supported by a Ph.D. fellowship from Consejo Nacional de Investigaciones Científicas y Técnicas (CONICET) to NGB and by research grants from the following institutions: Agencia Nacional de Promoción Científica y Tecnológica [PICT 2010-0128]; Universidad de Buenos Aires [2011-2014 X-481]; and CONICET [PIP 2009-2011N°112 200801 00519].

Acknowledgements

We thank Dr. Adrián Turjanski for helpful advice in the use of bioinformatic tools. We acknowledge the services of the proteomic core facility CEQUIBIEM (Facultad de Ciencias Exactas y Naturales, Universidad de Buenos Aires).

A. Supplementary material

Supplementary data associated with this article can be found, in the online version, at http://dx.doi.org/10.1016/j.jsb.2015.12.001.

References

Angelo, R., Rubin, C.S., 1998. Molecular characterization of an anchor protein (AKAPCE) that binds the RI subunit (RCE) of type I protein kinase A from Caenorhabditis elegans. J. Biol. Chem. 273, 14633–14643.

Banky, P., Huang, L.J., Taylor, S.S., 1998. Dimerization/docking domain of the type Ialpha regulatory subunit of cAMP-dependent protein kinase. Requirements for dimerization and docking are distinct but overlapping. J. Biol. Chem. 273, 35048–35055.

Banky, P., Roy, M., Newlon, M.G., Morikis, D., Haste, N.M., Taylor, S.S., Jennings, P.A., 2003. Related protein-protein interaction modules present drastically different surface topographies despite a conserved helical platform. J. Mol. Biol. 330, 1117–1129.

Benkert, P., Kunzli, M., Schwede, T., 2009. QMEAN server for protein model quality estimation. Nucleic Acids Res. 37, W510–514.

Boettcher, A.J., Wu, J., Kim, C., Yang, J., Bruystens, J., Cheung, N., Pennypacker, J.K., Blumenthal, D.A., Kornev, A.P., Taylor, S.S., 2011. Realizing the allosteric potential of the tetrameric protein kinase A RIalpha holoenzyme. Structure 19, 265–276.

Burgers, P.P., Ma, Y., Margarucci, L., Mackey, M., van der Heyden, M.A., Ellisman, M., Scholten, A., Taylor, S.S., Heck, A.J., 2012. A small novel A-kinase anchoring protein (AKAP) that localizes specifically protein kinase A-regulatory subunit I (PKA-RI) to the plasma membrane. J. Biol. Chem. 287, 43789–43797.

Canaves, J.M., Taylor, S.S., 2002. Classification and phylogenetic analysis of the cAMP-dependent protein kinase regulatory subunit family. J. Mol. Evol. 54, 17–29.

Carlson, G.L., Nelson, D.L., 1996. The 44-kDa regulatory subunit of the Paramecium cAMP-dependent protein kinase lacks a dimerization domain and may have a unique autophosphorylation site sequence. J. Eukaryot. Microbiol. 43, 347–356.

Cheng, J., Randall, A.Z., Sweredoski, M.J., Baldi, P., 2005. SCRATCH: a protein structure and structural feature prediction server. Nucleic Acids Res. 33, W72–76.

Cole, C., Barber, J.D., Barton, G.J., 2008. The Jpred 3 secondary structure prediction server. Nucleic Acids Res. 36, W197–201.

Comeau, S.R., Gatchell, D.W., Vajda, S., Camacho, C.J., 2004. ClusPro: a fully automated algorithm for protein-protein docking. Nucleic Acids Res. 32, W96–99.

Conrad, M., Schothorst, J., Kankipati, H.N., Van Zeebroeck, G., Rubio-Texeira, M., Thevelein, J.M., 2014. Nutrient sensing and signaling in the yeast *Saccharomyces cerevisiae*. FEMS Microbiol. Rev. 38, 254–299.

de Beer, T.A., Berka, K., Thornton, J.M., Laskowski, R.A., 2014. PDBsum additions. Nucleic Acids Res. 42, D292–296.

de Gunzburg, J., Veron, M., 1982. A cAMP-dependent protein kinase is present in differentiating Dictyostelium discoideum cells. EMBO J. 1, 1063–1068.

Erickson, H.P., 2009. Size and shape of protein molecules at the nanometer level determined by sedimentation, gel filtration, and electron microscopy. Biol. Proced. Online 11, 32–51.

Eswar, N., Webb, B., Marti-Renom, M.A., Madhusudhan, M.S., Eramian, D., Shen, M. Y., Pieper, U., Sali, A., 2006. Comparative protein structure modeling using Modeller. Curr. Protoc. Bioinform. (Chapter 5, Unit 5 6).

Franke, D., Svergun, D.I., 2009. DAMMIF, a program for rapid ab-initio shape determination in small-angle scattering. J. Appl. Crystallogr. 42, 342–346.

Galello, F., Moreno, S., Rossi, S., 2014. Interacting proteins of protein kinase A regulatory subunit in *Saccharomyces cerevisiae*. J. Proteomics 109C, 261–275.

Gancedo, J.M., 2013. Biological roles of cAMP: variations on a theme in the different kingdoms of life. Biol. Rev. Camb. Philos. Soc. 88, 645–668.

Garcia De La Torre, J., Huertas, M.L., Carrasco, B., 2000. Calculation of hydrodynamic properties of globular proteins from their atomic-level structure. Biophys. J. 78, 719–730.

Griffioen, G., Anghileri, P., Imre, E., Baroni, M.D., Ruis, H., 2000. Nutritional control of nucleocytoplasmic localization of cAMP-dependent protein kinase catalytic and regulatory subunits in *Saccharomyces cerevisiae*. J. Biol. Chem. 275, 1449–1456.

Griffioen, G., Branduardi, P., Ballarini, A., Anghileri, P., Norbeck, J., Baroni, M.D., Ruis, H., 2001. Nucleocytoplasmic distribution of budding yeast protein kinase A regulatory subunit Bcy1 requires Zds1 and is regulated by Yak1-dependent phosphorylation of its targeting domain. Mol. Cell Biol. 21, 511–523.

Hadad, M., Bresler-Musikant, T., Neuman-Silberberg, F.S., 2011. Drosophila spoonbill encodes a dual-specificity A-kinase anchor protein essential for oogenesis. Mech. Dev. 128, 471–482.

Hausken, Z.E., Coghlan, V.M., Hastings, C.A., Reimann, E.M., Scott, J.D., 1994. Type II regulatory subunit (RII) of the cAMP-dependent protein kinase interaction with A-kinase anchor proteins requires isoleucines 3 and 5. J. Biol. Chem. 269, 24245–24251.

Hixson, C.S., Krebs, E.G., 1980. Characterization of a cyclic AMP-binding protein from bakers' yeast. Identification as a regulatory subunit of cyclic AMP-dependent protein kinase. J. Biol. Chem. 255, 2137–2145.

Humphrey, W., Dalke, A., Schulten, K., 1996. VMD: visual molecular dynamics. J. Mol. Graph. 14 (33–38), 27–38.

Johnson, K.E., Cameron, S., Toda, T., Wigler, M., Zoller, M.J., 1987. Expression in Escherichia coli of BCY1, the regulatory subunit of cyclic AMP-dependent protein kinase from *Saccharomyces cerevisiae*. Purification and characterization. J. Biol. Chem. 262, 8636–8642.

Johnson, D.A., Akamine, P., Radzio-Andzelm, E., Madhusudan, M., Taylor, S.S., 2001. Dynamics of cAMP-dependent protein kinase. Chem. Rev. 101, 2243–2270.

Jones, S., 2012. Computational and structural characterisation of protein associations. Adv. Exp. Med. Biol. 747, 42–54.

Kelley, L.A., Sternberg, M.J., 2009. Protein structure prediction on the Web: a case study using the Phyre server. Nat. Protocol 4, 363–371.

Kinderman, F.S., Kim, C., von Daake, S., Ma, Y., Pham, B.Q., Spraggon, G., Xuong, N.H., Jennings, P.A., Taylor, S.S., 2006. A dynamic mechanism for AKAP binding to RII isoforms of cAMP-dependent protein kinase. Mol. Cell 24, 397–408.

Kozin, M.B., Svergun, D.I., 2001. Automated matching of high- and low-resolution structural models. J. Appl. Crystallogr. 34, 33–41.

Kronberg, F., Giacometti, R., Ruiz-Herrera, J., Passeron, S., 2011. Characterization of the regulatory subunit of Yarrowia lipolytica cAMP-dependent protein kinase. Evidences of a monomeric protein. Arch. Biochem. Biophys. 509, 66–75.

Li, Y., Rubin, C.S., 1995. Mutagenesis of the regulatory subunit (RII beta) of cAMP-dependent protein kinase II beta reveals hydrophobic amino acids that are essential for RII beta dimerization and/or anchoring RII beta to the cytoskeleton. J. Biol. Chem. 270, 1935–1944.

Matthews, J.M., Sunde, M., 2012. Dimers, oligomers, everywhere. Adv. Exp. Med. Biol. 747, 1–18.

McGuffin, L.J., Bryson, K., Jones, D.T., 2000. The PSIPRED protein structure prediction server. Bioinformatics 16, 404–405.

McWilliam, H., Li, W., Uludag, M., Squizzato, S., Park, Y.M., Buso, N., Cowley, A.P., Lopez, R., 2013. Analysis Tool Web Services from the EMBL-EBI. Nucleic Acids Res. 41, W597–600.

Mertens, H.D., Svergun, D.I., 2010. Structural characterization of proteins and complexes using small-angle X-ray solution scattering. J. Struct. Biol. 172, 128–141.

Mutzel, R., Lacombe, M.L., Simon, M.N., de Gunzburg, J., Veron, M., 1987. Cloning and cDNA sequence of the regulatory subunit of cAMP-dependent protein kinase from Dictyostelium discoideum. Proc. Natl. Acad. Sci. USA 84, 6–10.

Mylonas, E., Svergun, D.I., 2007. Accuracy of molecular mass determination of proteins in solution by small-angle X-ray scattering. J. Appl. Crystallogr. 40, 245–249.

Newlon, M.G., Roy, M., Morikis, D., Hausken, Z.E., Coghlan, V., Scott, J.D., Jennings, P. A., 1999. The molecular basis for protein kinase A anchoring revealed by solution NMR. Nat. Struct. Biol. 6, 222–227.

Paveto, C., Passeron, S., Corbin, J.D., Moreno, S., 1989. Two different intrachain cAMP sites in the cAMP-dependent protein kinase of the dimorphic fungus Mucor rouxii. Eur. J. Biochem. 179, 429–434.

Peng, M., Aye, T.T., Snel, B., van Breukelen, B., Scholten, A., Heck, A.J., 2015. Spatial Organization in Protein Kinase A Signaling Emerged at the Base of Animal Evolution. J. Proteome Res. 14, 2976–2987.

Pidoux, G., Tasken, K., 2010. Specificity and spatial dynamics of protein kinase A signaling organized by A-kinase-anchoring proteins. J. Mol. Endocrinol. 44, 271–284.

Portela, P., Zaremberg, V., Moreno, S., 2001. Evaluation of in vivo activation of protein kinase A under non-dissociable conditions through the overexpression of wild-type and mutant regulatory subunits in *Saccharomyces cerevisiae*. Microbiology 147, 1149–1159.

Receveur-Brechot, V., Durand, D., 2012. How random are intrinsically disordered proteins? A small angle scattering perspective. Curr. Protein Pept. Sci. 13, 55–75.

Rinaldi, J., Wu, J., Yang, J., Ralston, C.Y., Sankaran, B., Moreno, S., Taylor, S.S., 2010. Structure of yeast regulatory subunit: a glimpse into the evolution of PKA signaling. Structure 18, 1471–1482.

Rodrigues, J.P., Levitt, M., Chopra, G., 2012. KoBaMIN: a knowledge-based minimization web server for protein structure refinement. Nucleic Acids Res. 40, W323–328.

Sarma, G.N., Kinderman, F.S., Kim, C., von Daake, S., Chen, L., Wang, B.C., Taylor, S.S., 2010. Structure of D-AKAP2:PKA RI complex: insights into AKAP specificity and selectivity. Structure 18, 155–166.

Schneidman-Duhovny, D., Hammel, M., Sali, A., 2010. FoXS: a web server for rapid computation and fitting of SAXS profiles. Nucleic Acids Res. 38, W540–544.

Schneidman-Duhovny, D., Kim, S.J., Sali, A., 2012. Integrative structural modeling with small angle X-ray scattering profiles. BMC Struct. Biol. 12, 17.

Sherman, F., Fink, G.R., Hicks, J.B., 1986. Laboratory Course Manual for Methods in Yeast Genetics. Cold Spring Harbor Laboratory, NY.

Siegel, L.M., Monty, K.J., 1966. Determination of molecular weights and frictional ratios of proteins in impure systems by use of gel filtration and density gradient centrifugation. Application to crude preparations of sulfite and hydroxylamine reductases. Biochim. Biophys. Acta 112, 346–362.

Su, Y., Dostmann, W.R., Herberg, F.W., Durick, K., Xuong, N.H., Ten Eyck, L., Taylor, S. S., Varughese, K.I., 1995. Regulatory subunit of protein kinase A: structure of deletion mutant with cAMP binding domains. Science 269, 807–813.

Svergun, D.I., 1992. Determination of the regularization parameter in indirect-transform methods using perceptual criteria. J. Appl. Crystallogr. 25, 495–503.

Tasken, K., Aandahl, E.M., 2004. Localized effects of cAMP mediated by distinct routes of protein kinase A. Physiol. Rev. 84, 137–167.

Taylor, S.S., Kim, C., Vigil, D., Haste, N.M., Yang, J., Wu, J., Anand, G.S., 2005. Dynamics of signaling by PKA. Biochim. Biophys. Acta 1754, 25–37.

Toda, T., Cameron, S., Sass, P., Zoller, M., Scott, J.D., McMullen, B., Hurwitz, M., Krebs, E.G., Wigler, M., 1987. Cloning and characterization of BCY1, a locus encoding a regulatory subunit of the cyclic AMP-dependent protein kinase in *Saccharomyces cerevisiae*. Mol. Cell Biol. 7, 1371–1377.

Trevillyan, J.M., Pall, M.L., 1982. Isolation and properties of a cyclic AMP-binding protein from Neurospora. Evidence for its role as the regulatory subunit of cyclic AMP-dependent protein kinase. J. Biol. Chem. 257, 3978–3986.

Vigil, D., Blumenthal, D.K., Brown, S., Taylor, S.S., Trewhella, J., 2004a. Differential effects of substrate on type I and type II PKA holoenzyme dissociation. Biochemistry 43, 5629–5636.

Vigil, D., Blumenthal, D.K., Heller, W.T., Brown, S., Canaves, J.M., Taylor, S.S., Trewhella, J., 2004b. Conformational differences among solution structures of the type Ialpha, IIalpha and IIbeta protein kinase A regulatory subunit homodimers: role of the linker regions. J. Mol. Biol. 337, 1183–1194.

Volkov, V.V., Svergun, D.I., 2003. Uniqueness of ab initio shape determination in small-angle scattering. J. Appl. Crystallogr. 36, 860–864.

Welch, E.J., Jones, B.W., Scott, J.D., 2010. Networking with AKAPs: context-dependent regulation of anchored enzymes. Mol. Interv. 10, 86–97.

Yachdav, G., Kloppmann, E., Kajan, L., Hecht, M., Goldberg, T., Hamp, T., Honigschmid, P., Schafferhans, A., Roos, M., Bernhofer, M., Richter, L., Ashkenazy, H., Punta, M., Schlessinger, A., Bromberg, Y., Schneider, R., Vriend, G., Sander, C., Ben-Tal, N., Rost, B., 2014. PredictProtein–an open resource for online prediction of protein structural and functional features. Nucleic Acids Res. 42, W337–W343.

Please cite this article in press as: González Bardeci, N., et al. The PKA regulatory subunit from yeast forms a homotetramer: Low-resolution structure of the N-terminal oligomerization domain. J. Struct. Biol. (2015), http://dx.doi.org/10.1016/j.jsb.2015.12.001